Surging Wind Turbine Simulations with a Free Wake Panel Method

Ribeiro, A. F.P.; Casalino, D.; Ferreira, C. S.

DOI
10.1088/1742-6596/2265/4/042027

Publication date
2022

Document Version
Final published version

Published in
Journal of Physics: Conference Series

Surging Wind Turbine Simulations with a Free Wake Panel Method

Surging Wind Turbine Simulations with a Free Wake Panel Method

A F P Ribeiro, D Casalino and C S Ferreira
Delft University of Technology, Delft, the Netherlands
E-mail: a.pintoribeiro@tudelft.nl

Abstract. We investigate the aerodynamics of a surging wind turbine with numerical simulations based on a free wake panel method. We start by demonstrating the method's capability to simulate a plunging airfoil, which provides some insights that are later used to interpret results of a surging rotor. We then validate the method on a non-surging wind turbine and discuss the strengths and weaknesses of our approach. Next, we focus on the UNAFLOW case: a surging wind turbine which was modelled experimentally and with various numerical methods. Good agreement with experimental data is observed for amplitude and phase of the thrust with surge motion. For the first time, we achieve numerical results of a wind turbine wake that accurately reproduce experimentally verified effects of surging motion. Finally, we extend our simulations beyond the frequency range of the UNAFLOW experiments and reach results that do not follow a quasi-steady response. Using the plunging airfoil data, we justify the behavior observed in the non-linear range. Our work seeks to contribute a different method to the pool of results for the UNAFLOW case, while extending the analysis to conditions that have not been simulated before.

1. Introduction

With the wind energy market leaning heavily towards offshore turbines in recent years, floating wind turbines have become the focus of significant research. One of the many challenges of such configurations is that, due to oceanic waves, the turbine is subjected to large amplitude motions, making its aerodynamics even more complex than that of onshore turbines. The UNAFLOW [1, 2] project provided a simplified test case for a non-stationary rotor, by simulating a surging wind turbine in a wind tunnel, without any tilting of the tower. Several groups have simulated the UNAFLOW case with different methodologies including blade element momentum theory (BEM), lifting line, and computational fluid dynamics (CFD), with fairly good results being achieved [3, 4, 5].

In this work, we seek to contribute to this pool of results by simulating the UNAFLOW case with a source and doublet free wake panel method. Unlike BEM and lifting line, panel methods directly model the blades, free from table look ups, while still being a fraction of the cost of a CFD simulation [6]. They can also include blade thickness effects, by simulating the entire blade surface, rather than the camber surface or a single line, which can lead to better accuracy [7]. Panel methods have also been shown to accurately model full rotors, including aeroelastic effects [8, 9, 10]. The free wake allows for complex scenarios, such as blade vortex interaction [11], which could happen in extreme surge conditions.

With these characteristics in mind, this is an important stepping stone towards the ultimate goal of this research: aeroelastic simulations of floating off-shore wind turbines through a fully-coupled transient aerodynamic/structural fluid-structure interaction (FSI). To our knowledge, only experimental and CFD results have been used to investigate the wake of the UNAFLOW turbine [3]. CFD adds significant diffusion to the tip vortices, making comparisons to experiments difficult. Hence, in this work we also show how the free wake panel method compares to experimental measurements of the wake.

The panel method shown here was created with the intent to be faster than available methods by use of efficient algorithms and modern acceleration techniques, such as leveraging GPUs for the calculations. At the moment, our implementation was compared to an open source C++ panel code [12] and we observed over an order of magnitude in speed up. Our code will also be coupled to Simpack, a state-of-the-art multi-body dynamics solver.

In the following sections, we first verify and validate our method by simulating a plunging airfoil and a non-surging wind turbine. We then turn to the UNAFLOW rotor and simulate different surging conditions by changing the frequency and amplitude of the rotor surging motion. Results are compared to experimental data and the discrepancies are discussed.

2. Methodology

We employ a source and doublet panel method with free-wakes [13] in order to capture the aerodynamics of the surging wind turbine rotor. The thickness effects are fully captured, as the panels lie on the blades surfaces. Blade-vortex interaction capabilities [11] are implemented, but not used for this study, as the turbine does not cross its own wake. The surface and wake discretization of the velocity potential equation leads to the following linear system:

$$\frac{1}{4\pi}A_{ij}\mu_j + \frac{1}{4\pi}B_{ij}\sigma_j + \frac{1}{4\pi}C_{iw}\gamma_w = 0 \tag{1}$$

where A, B, and C are the influence coefficients matrices [14] for the doublets μ, sources σ, and wake vortices γ respectively. The values of μ, σ, and γ are constant over each panel. A far-field formulation can be used to make the calculations of the influence coefficients substantially faster when computing A, B, and C over large distances [14]. The sources σ are computed to ensure impermeability, with:

$$\sigma = -(\vec{U}_\infty - \vec{U}_k) \cdot \hat{n} \tag{2}$$

where $\vec{U}_\infty$ is the freestream velocity, $\vec{U}_k$ is the kinematic velocity of the surface panels, and $\hat{n}$ is the surface normal. The wake vortices can be computed based on the doublets intensities on the top (t) and bottom (b) of the trailing edge, following the Kutta condition:

$$\gamma = \mu^t - \mu^b - (\Phi^t_\infty - \Phi^b_\infty) \tag{3}$$

where $\Phi_\infty = \vec{U}_\infty \cdot \vec{x}$ is the freestream potential at an arbitrary location $\vec{x}$, which in this case are the center of the top and bottom panels. The term in parentheses is often neglected, but is critical when simulating thick geometries using coarse meshes [15], as wind turbines blades roots. Combining Equations , 2, and 3, we are left with a square linear system with the doublets μ as unknowns. We solve this system either by direct matrix inversion or by the generalized minimal residual method (GMRES).

When symmetries are present, as in turbines with multiple blades and no yaw, virtual bodies across symmetry planes or axes can be used [13], which dramatically reduce the influence coefficients matrices. With the linear system solved, surface velocities $\vec{U}$ are computed based on the basic potential flow equation, $\vec{U} = -\nabla\Phi$, where Φ is the velocity potential. The surface gradient is computed with central differences for quadrangular panels, but a least squares

approximation [16, 17] is also available, and is always used for triangular panels. With the surface velocity available, the unsteady Bernoulli equation [18] is used to find the surface pressure, which is then integrated over all surface panels to find the forces and moments acting on the bodies. The time derivatives in the unsteady Bernoulli equation is calculated with a first order backwards Euler method.

At every timestep, wake vortices are convected due to the freestream velocity and the induction of all the surface and wake panels. We take special care of the first vortices after the trailing edge, which are shown in 2D in Figure 1. Three vortices are shown, with coordinates $\vec{w}_i$. The first vortex is attached to the blade trailing edge. From the second row onwards, the vortices are free to be convected as each timestep passes. The translation from the first row to the second row of wake filaments is assumed to be dragged closer to the trailing edge by a certain factor W, which typically multiplies the assumed distance the vortex would travel in one timestep $\vec{U}_\infty \Delta t$ by $0.2 - 0.3$ [13]. However, it is not easy to justify that the velocity at the trailing edge equals the freestream in magnitude and direction. In the current implementation, when the first vortex is moved to the second row, it is placed on a parabola that is aligned with the bisection of the trailing edge and connected to the trailing edge and the next free vortex (which is now $\vec{w}_3$). The factor W is used as a ratio of the distance between the trailing edge (the new $\vec{w}_1$) and $\vec{w}_3$. The choice of making the parabola parallel to the bisection of the trailing edge, instead of parallel to the bottom panel was made keeping in mind that sometimes blunt trailing edges (such as those found in real geometries) are turned into a cusp (as required by this panel method) by abruptly beveling the top and bottom surfaces.

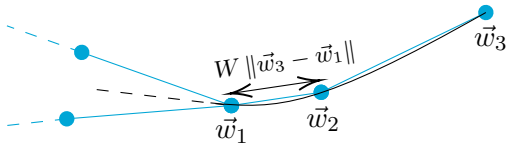

Figure 1. First three rows of wake vortices. Dashed black line is the bisection of the trailing edge cusp. Solid black line is a parabola.

3. Code Verification: Plunging Airfoil

We perform simulations of a NACA0001 airfoil under plunging conditions, where the vertical position h oscillates as a sinusoidal function of time, with an amplitude of 1% of the chord c and a reduced frequency $k = \omega c / 2U_\infty$, where ω is the oscillation angular frequency. Such simulations can be verified with the Theodorsen [19] analytical solution, which also uses the assumptions of potential flow. Hence, results should be nearly identical between simulations and theory, therefore we consider this a verification of the code. Results for the amplitude of the lift coefficient oscillations ΔC_L and phase of the vertical velocity with respect to the vertical position $\phi_{C_L,h}$ are shown in Figures 2 and 3, respectively. A timestep (Δt) study is shown, where we vary the number of timesteps in an oscillation period T.

Very good agreement between the simulations and the Theodorsen solution can be observed for all values of k. Around $k < 1$ we observe discrepancies of a few degrees in the phase angle when we use 20 timesteps per period, with 40 and 80 timesteps per period matching Theodorsen very well. In contrast, ΔC_L seems largely unaffected by Δt.

4. Code Validation: NREL Phase VI Wind Turbine

The NREL Phase VI 15 kW turbine [20][21] is used for validation of the method for wind turbines. The experiments for this turbine include pressure coefficient (Cp) cuts on the blades,

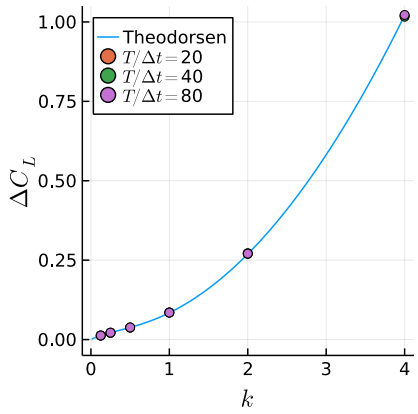

Figure 2. Amplitude of lift coefficient oscillations vs reduced frequency for plunging airfoil.

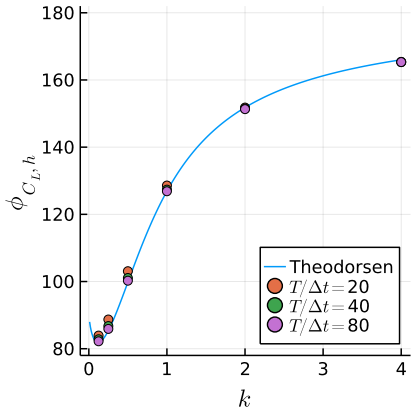

Figure 3. Phase of lift coefficient with respect to vertical position vs reduced frequency for plunging airfoil.

allowing for a more detailed comparison to simulations than using integral quantities, such as thrust and torque. This case presents a realistic blade geometry and is challenging for a fully inviscid panel code, as it deals with a highly loaded thick airfoil (the S809), with significant flow separations in the root. Therefore, some inaccuracies are to be expected.

Simulations are run with uniform flow, with $U_\infty = 7$ m/s and rotor angular velocity of 72 RPM. The rotor radius is 5.029 m and the turbine has two blades. A very fine block structured surface mesh with about 42,000 elements, used in several CFD studies in the past [22][23], is employed for this case, as it provides a detailed representation of the blade tips. This mesh is substantially finer than what is typically used in panel codes. We use 60 timesteps per revolution, simulating 20 revolutions total. Only one of the two blades is simulated, with axial symmetry being used to speed up the simulations. This can be observed in Figure 4, which also shows the large number of rotations simulated and highly tangled wake panels at the very end of the wake. This forces us to avoid the far-field influence coefficients calculations mentioned in Section 2. Using the far-field formulation for this case, although significantly cheaper, led to unphysical fluctuations on the wake and on the blade surface as the wake panels moved far away from the blades and the far-field formulation was activated. This is because the tangled panels violate the flatness assumption of the far-field formulation.

Figure 5 shows the Cp distributions along position x over the local chord c at three planes across the blade, showing good agreement with experimental data. Some differences are seen in the root section, near the trailing edge, which occur due to the separated flow that should occur in the root region. Closer to the center of the blade, suction peaks are overpredicted, as expected from a fully inviscid simulation. Towards the blade tip, the airfoil is less loaded and a good match with experiments can be found. Hence, Figure 5 highlights the high accuracy this method can achieve, while also showing the limitations of the current fully inviscid implementation.

5. Surging Wind Turbine Simulations

The UNAFLOW turbine case [2] consists of a 3 blade rotor with a diameter of 2.38 m, rotating at 150 to 265 RPM, with U_∞ between 2.5 and 6 m/s. The entire rotor surges upwind and downwind at a frequency (f) ranging from 0.125 to 2 Hz and amplitude (A) from 2.5 to 125 mm. This motion is performed such that the rotation axis is always aligned with the freestream, meaning no yawed flow occurs. As the majority of the experimental data are for $U_\infty = 4$ m/s

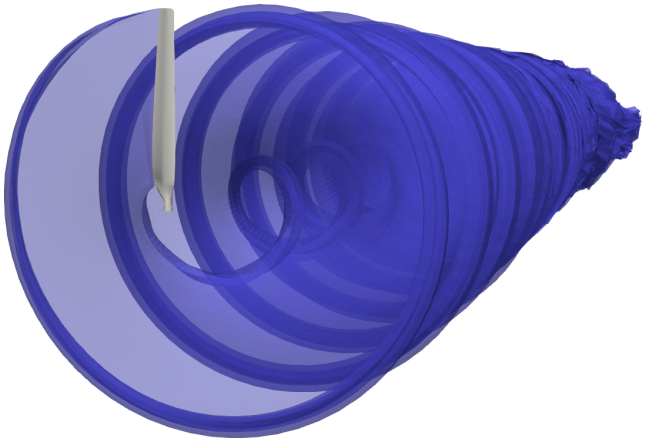

Figure 4. Blade and wake of the NREL Phase VI simulation. Second blade and its wake are modelled with axial symmetry.

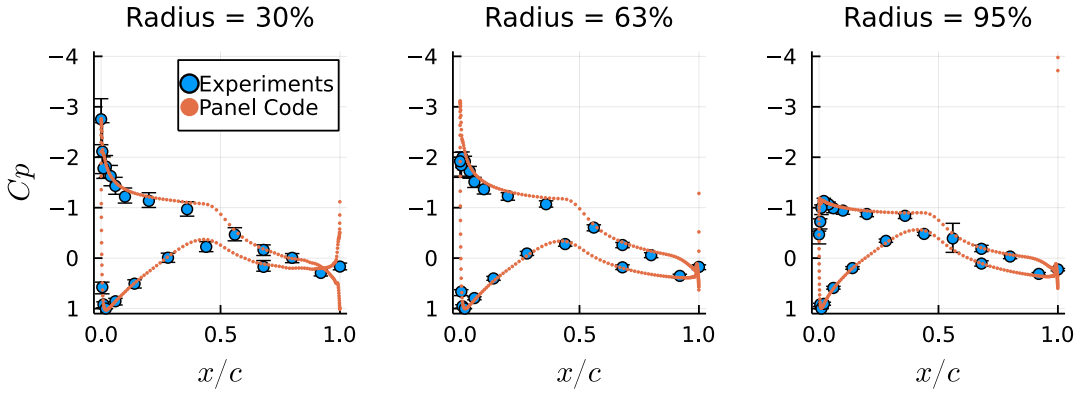

Figure 5. Pressure coefficient in different planes along the NREL Phase VI blade compared to experiments.

and RPM of 241, these are the conditions we simulate in this work. We use different values of f and A for our simulations, based on availability of experimental data, while giving a preference to cases with high surge velocity.

The surge velocity $U_S = 2\pi f A$ is the maximum rotor translation velocity, relative to the ground and is mostly limited to 0.2 m/s or $U_S/U_\infty = 0.05$ in the experiments. Such modest values mean large non-linear results are not to be expected, as we will see in the next sections. Although simulations are done in model scale, in order to get a better sense of the case, it is useful to scale up these values to a realistic wind turbine. The full scale version of the UNAFLOW model, the DTU 10MW turbine, is 75 times larger and encounters flow speeds 6 times larger, with a diameter of 180 m, $U_\infty = 24$ m/s, and 9.6 RPM [24]. With $f = 0.16$ Hz, for the same $U_S/U_\infty = 0.05$ this corresponds to $A = 1.2$ m and $U_S = 1.2$ m/s.

The blades are based on the SD7032 airfoil section, transitioning into a circle in the root region. For the simulations in this work, the blade geometry was constructed based on chord and twist distributions provided in the experimental data set [25]. However this led to small differences in the geometry. In particular, the blade chord approaches zero at the tip [24], which is inconsistent with the geometry description [25], and can lead to some differences in results. Figure 6 shows the UNAFLOW wind turbine, along with its wake, as simulated by the methods

described in this paper. The blades are simulated without the hub and tower for simplicity.

Figure 6. Panel method simulation results of the UNAFLOW rotor and its wake.

The blades are discretized with 100 chordwise panels, using a cosine distribution, and 50 equally spaced spanwise panels each, with a total of about 15 thousand panels. The panel distribution is shown in Figure 7. This panel distribution was chosen as it provided grid converged results for several preliminary studies on airfoils and rotors, not included here for brevity. The timestep is set to 1/36 of a revolution unless otherwise stated, which corresponds to a rotation angle of $\Delta\psi = 10°$. Simulations are run for at least 40 revolutions, leading to about 216 thousand wake panels. This time discretization corresponds to 72 timesteps per surging period for $f = 2$ Hz, which is the highest surge frequency available in the experimental data set.

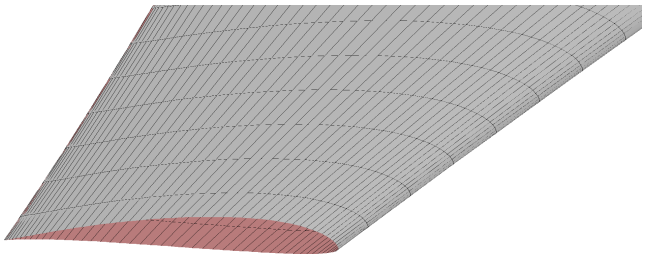

Figure 7. Surface mesh used for the UNAFLOW blade, cut by a clipping plane.

5.1. Timestep study

As in Section 3, we begin with a timestep study, which can also be seen as a study on the wake refinement. This was achieved by first using values of $\Delta\psi$, or rotation angle per timestep of 20, 10, and 5°. We perform this study for $f = 2$ Hz and $A = 15$ mm.

The time history of the thrust coefficient (C_T) is shown in Figure 8, which includes experimental data (filtered at the surge frequency with a Fourier transform, as it originally includes substantial noise), along with numerical results with the three different timesteps mentioned in the previous paragraph. Simulations are run for 10 seconds, or 40 revolutions, or 20 surge cycles for $f = 2$ Hz. The simulations shown appear converged in terms of mean and unsteady components of thrust, with the $\Delta\psi = 5°$ results being quite close to $\Delta\psi = 10°$. Results are shown up to 6 seconds for clarity, but simulations are run for 10 seconds. Overall, we consider these results adequate for the statistical analysis that follows. In the following simulations, we analyse our data from time $t = 5$ to $t = 10$ seconds.

A quantitative analysis can be seen in Figure 9, which shows the mean thrust and power (C_P) coefficients variation with $\Delta\psi$. The timestep study indicates that C_T is sensitive to the time (or wake) discretization. However, C_T results are consistent, with shorter timesteps leading to better accuracy and a convergent behavior being observed. Using the Richardson extrapolation [26] on our results would lead to C_T within 0.7% of experimental values. The $\Delta\psi = 10°$ result is within 0.7% of the extrapolation, justifying our choice of $\Delta\psi = 10°$. I contrastto C_T, C_P is substantially higher than experimental values, shows a flatter trend, and is not monotonic. However, this is not surprising, as C_P is sensitive to sectional drag, which the inviscid method herein does not capture.

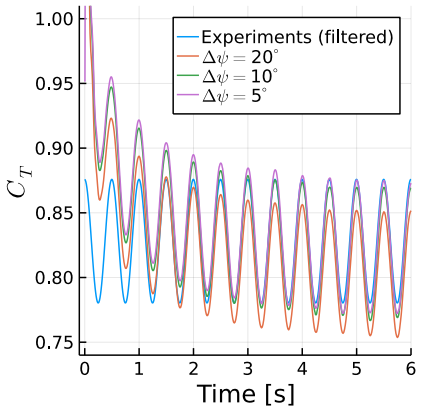

Figure 8. Time history of thrust coefficient for various timesteps, compared to experimental data. Time shown up to 6 seconds, full simulation is 10 seconds.

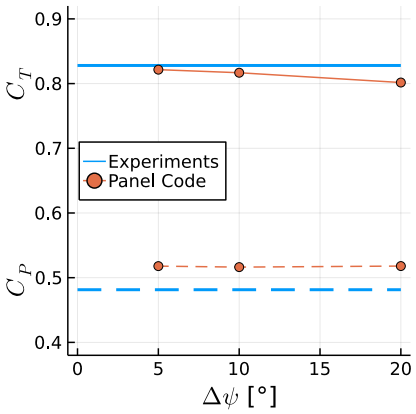

Figure 9. Timestep effect on the power (dashed lines) and thrust (solid lines) coefficients.

5.2. Surge velocity effects

Here, we expand on the previous simulation results by examining the fluctuating component of C_T. While keeping $A = 15$ mm, we vary f between 0 and 2 Hz. Figure 10 shows the effect of U_S/U_∞ on the amplitude of the fluctuations of thrust (ΔC_T). The convergence of ΔC_T with $\Delta\psi$ is not shown for brevity, but it behaves in a very similar way to the convergence of C_T. Figure 11 shows the effect of U_S/U_∞ on the phase shift ϕ between the rotor position and the fluctuations of C_T. Once again, the experimental data was filtered at the surge frequency. The lowest surge frequency, $f = 0.5$ Hz was run for twice as long as other cases, to obtain meaningful statistics from the simulations.

The values of ΔC_T agree well with experimental data, with an approximately linear relation between the surge velocity and the thrust fluctuations. This confirms the quasi-steady nature of the results, which is likely due to the relatively small values of U_S [27]. The average slope of ΔC_T as a function of U_S/U_∞ in the simulations is 15% higher than in the experiments, potentially due to the inviscid approach. The values of ϕ fall within the experimental scatter, being within 3° of −90° for all cases, which corresponds to the quasi-steady response.

5.3. Rotor wake

We now focus on the rotor wake. The UNAFLOW experiments included particle image velocimetry (PIV) on a vertical plane in the rotor wake, aligned with the center of the nacelle. Measurements were made at several stages of the surging motion and averaged over several

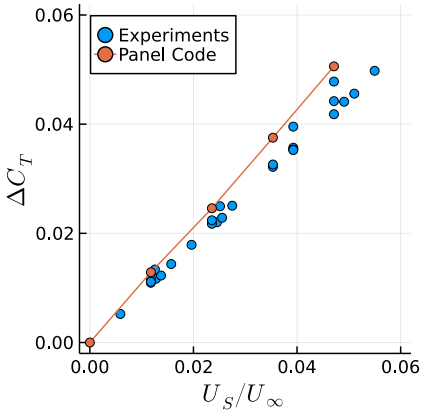

Figure 10. Maximum surge velocity effect on the amplitude of the fluctuation of the thrust coefficient. Simulations at constant A, experiments at various A shown.

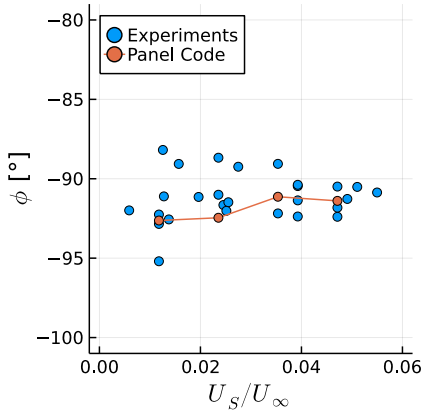

Figure 11. Maximum surge velocity effect on the phase between the rotor position and its thrust. Simulations at constant A, experiments at various A shown.

snapshots, with the rotor always being in the same azimuth [2]. We focus on two rotor positions, which the experiments refer to as steps 1 and 5. Both steps correspond to the rotor being in its central position ($x=0$), with the rotor moving with maximum velocity against the wind in step 1 ($\dot{x}=-U_S$) and maximum velocity with the wind in step 5 ($\dot{x}=U_S$). As the rotor is in the same position and same azimuth for both steps, any change in the wake is caused by unsteady effects of the surging motion.

Simulations are done with $f=1$ Hz and $A=35$ mm, which corresponds to $U_S/U_\infty=0.055$, the highest value shown in the previous section. This configuration was selected since it contains PIV data for all steps, while also having a high value of U_S. Figure 12 shows the UNAFLOW rotor, along with the wake panels and the PIV plane, as a reference for the results discussed in the following paragraphs. When the rotor crosses steps 1 and 5, the bottom blade is rotated 187° away from the PIV plane.

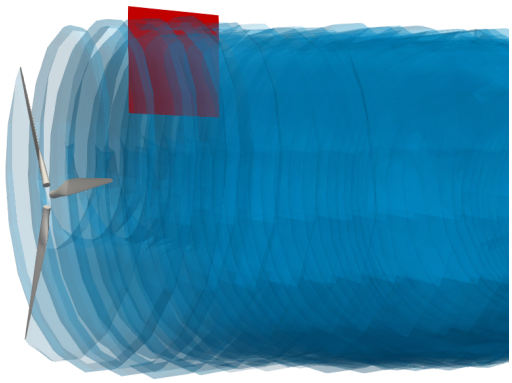

Figure 12. UNAFLOW wind turbine (grey), wake panels (blue), and PIV plane (red).

Figures 13 and 14 show experimental and numerical results on the PIV plane. Both steps 1 and 5 are shown in each figure, in order to better see the difference between them. Consistent with expectations, during step 1 the tip vortices are further downstream than in step 5. The

horizontal distance between the vortices in steps 1 and 5 is about 6 cm in both simulations and experiments. The vortices radial position is noticeably different, likely in large part due to the blades tip geometry not being identical to the experimental blades, as they are not described in details in the documentation. The blades in the simulations are slightly longer and have a larger chord on the tip. Other factors that can contribute to the differences are the wake discretization and the neglected viscosity, which plays a role in the creation of the tip vortices.

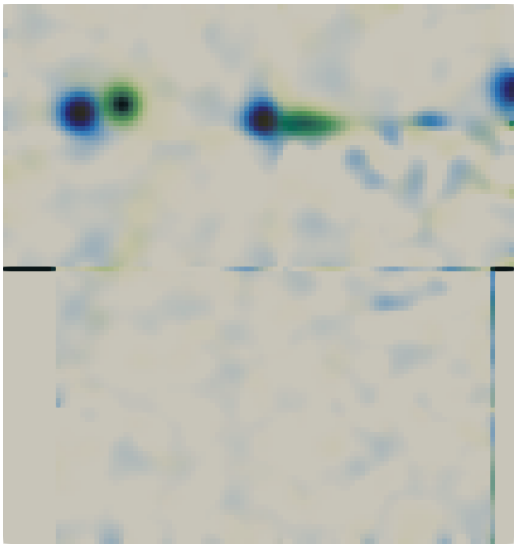

Figure 13. Experimental tip vortex position on steps 1 (green) and 5 (blue). Vorticity perpendicular to the plane shown from 0 to 300 1/s.

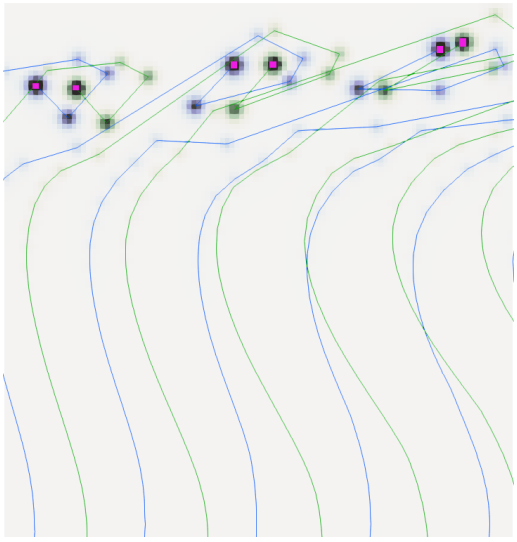

Figure 14. Numerical wake on steps 1 (green) and 5 (blue). Vorticity perpendicular to the plane shown from 0 to 300 1/s. Lines represent a cut through the wake panels. Pink dots highlight the tip vortices.

CFD simulations conducted for the UNAFLOW turbine [3] were able to capture the horizontal displacement of the first tip vortex in Figures 13 and 14 to some extent. However, the second tip vortex displacement was inverted, that is, the vortex from step 1 was upstream of the position in step 5. To our knowledge, no other studies have been made where the wake of a surging wind turbine was simulated numerically and the results were validated with experiments. Hence, we believe this is the first time that a surging wind turbine simulation shows results that agree well with experimental data in terms of wake dynamics.

The results in Figure 14 also highlight the discrete nature of the simulation. The wake does not consist of a smooth vorticity distribution and is instead represented by discrete filaments, which are seen as numerous individual vortices on the plane. For comparison with experimental data, it is easier to ignore the small vortices and focus on the largest ones, which correspond to the tip vortices. They are highlighted with pink dots in the image, for clarity. As is usually the case with discrete methods, refining the wake panels would lead to smoother distributions, at the cost of higher computational time. In the case of this vertical plane, this would mean refining the blades in the spanwise direction, particularly near the blade tips.

Finally, it is worth noting that the wind turbine wake is folding upon itself on the right side of Figure 14. This is a common consequence of using an inviscid free wake method, as complex wakes tend to become tangled as they develop, which can be partially observed on the right side of Figure 6. Using a vortex core model [28] can stabilize the wake for a longer time if the vortex core radius is large enough, but has small effects on the location of the tip vortices in the

plane investigated here. The UNAFLOW rotor shows more tangling near the turbine than the NREL Phase VI due to higher RPM, higher blade count, and lower U_∞, leading to the wakes of the different blades being much closer to each other. In both cases, the simulations shown here employed the aforementioned vortex core model and achieved better wake stability with it.

5.4. Beyond the UNAFLOW Results

Looking beyond the UNAFLOW experiments, where U_S/U_∞ was limited by experimental constraints, we can investigate the effects of stronger surging motion. Let us assume $f = 10$ Hz and $A = 100$ mm, which leads to $U_S/U_\infty = 1.5$. Let us also make the unlikely assumption of no dynamic stall. Considering the local flow velocity as the vector sum of the freestream velocity and the rotation velocity, the reduced frequency on the entire blade is under $k = 0.4$. Theodorsen results in Figure 3 show rapid changes in the phase angle for small values of k, meaning even very slow oscillations show some hysteresis effects. However, Figure 2 shows only a modest increase in lift with small values of k. One can see a superlinear increase in ΔC_L only when $k > 1$, which is very high for a wind turbine [29], as even scaling the UNAFLOW experiments to the full scale would still lead to $k < 0.2$ over the entire blade.

This leads us to the conclusion that we should not expect a superlinear increase in ΔC_T with increasing U_S from Theodorsen effects, but instead, should encounter a decrease in ΔC_T, as different sections of the blade with different values of k would be out of phase with each other. With large U_S, blades would reach dynamic stall and, in extreme surge conditions, would cross their own wakes. These obviously lead to non-linear effects and could be the topic of future studies. Here, we seek to quantify the Theodorsen effects for stronger surge motion. Hence, we limit ourselves to attached flows, which is appropriate for the inviscid panel method, and investigate the effects of $U_S/U_\infty > 0.05$ or $f > 2$ Hz, while keeping A small, so no strong interactions with the wake occur.

Results for these simulations are shown in Figures 15 and 16. The orange circles represent the data shown in Section 5.2, with $A = 0.015$ mm and f varying between 0.5 and 2 Hz. The green circles show an extension of the orange data, with the same A, but with f varying from 2 to 8 Hz. The purple circle shows a single result, at $A = 0.05$ mm and $f = 1$ Hz. The grey dashed line in Figure 15 is a linear extension of the orange circles. The grey region in Figure 16 represents the quasi-steady regime, which we set around $-90° \pm 3°$, as this contains most of the experimental data.

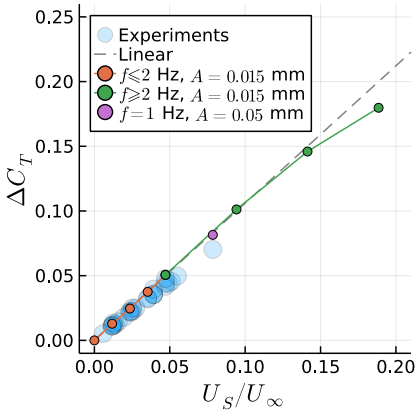

Figure 15. Maximum surge velocity effect on the amplitude of the fluctuation of the thrust coefficient.

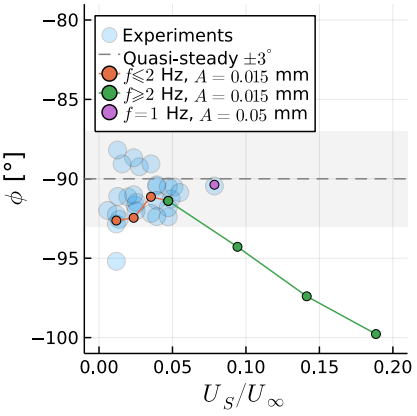

Figure 16. Maximum surge velocity effect on the phase between the rotor position and its thrust.

We can now find where ΔC_T breaks from a linear trend and when ϕ leaves the quasi-steady regime. At $f = 6$ Hz or $U_S/U_\infty = 0.14$, we observe a noticeable deviation from the linear relation between ΔC_T and U_S. As postulated in this section, the effect of increasing U_S leads to a reduction in ΔC_T, instead of the increase seen in 2D. In contrast ϕ moves away from the quasi-steady regime at an earlier point, near $f = 4$ Hz or $U_S/U_\infty = 0.09$.

We also see in Figure 16 experimental and numerical data at $A = 0.05$ mm and $f = 1$ Hz, or $U_S/U_\infty = 0.08$. Although U_S/U_∞ is relatively high for this case, the response is still quasi-steady. This is consistent with the other results shown here, as this case still has the same k as the orange circle at $U_S/U_\infty = 0.02$ and hence, the Theodorsen effects are small. Thus, for cases beyond the linear quasi-steady response, ϕ should be shown against f, assuming constant U_∞, RPM, and rotor geometry. For a discussion on how to normalize surging rotor data, including ΔC_T, see [27]. Note that the reduced frequency used in [27] does not include the RPM, which is an important component of the velocity along the blade, highly affecting k. We believe a more general approach to normalize f should include RPM.

6. Summary and Next Steps

We have shown that a free wake panel method can accurately capture mean and unsteady thrust of a surging wind turbine. The methodology used in this paper slightly underpredicts the mean thrust and overpredicts the amplitude of thrust fluctuations, however results are comparable and in line with the state-of-the-art [27].

The effects of the rotor motion on the tip vortices was also shown to be accurately captured by the method in what we believe is the first publication of surging wind turbine wakes that accurately reproduce experimental data. Wake vortices are particularly difficult to capture with CFD methods, as the Eulerian approach tends to dissipate them [3]. Lagrangian methods have a significant advantage in preserving the wake vortices near the body, with the disadvantage of wake entanglement far from the rotor, which in turn requires some dissipation for stabilization.

Finally, we found that the surge velocity had to be tripled from its maximum value in the experimental campaign to reach a non-linear response in thrust. The current method allowed us to investigate this by isolating Theodorsen effects. This means that, in reality, the non-linear response could happen earlier due to other phenomena, such as dynamic stall. By investigating k along the wind turbine blades and comparing to 2D results, we postulate that the changes in thrust are mostly related to changes in phase, as sections along the blade are out of phase with each other. This explains why thrust is reduced, instead of increased as in 2D sections.

This work is a stepping stone towards building a tool that is able to simulate floating offshore wind turbines in a way that is accurate, robust, and efficient. Future work will expand to more complex cases, such as full offshore platform motion and aeroelasticity.

Acknowledgments

The authors are grateful to Felipe Miranda for providing the experimental data [25]. We are also very grateful for the help of Massimo Gennaretti and Riccardo Giansante in achieving accurate results for the Theodorsen case.

References

[1] Bayati I, Bernini L, Zanotti A, Belloli M and Zasso A 2018 *Journal of Physics: Conference Series* **1037** 052024 URL `https://doi.org/10.1088/1742-6596/1037/5/052024`

[2] Fontanella A, Bayati I, Mikkelsen R, Belloli M and Zasso A 2021 *Wind Energy Science* **6** 1169–1190 URL `https://wes.copernicus.org/articles/6/1169/2021/`

[3] Bayati I, Belloli M, Bernini L, Boldrin D, Boorsma K, Caboni M, Cormier M, Mikkelsen R, Lutz T and Zasso A 2018 *Journal of Physics: Conference Series* **1037** 072037 URL `https://doi.org/10.1088/1742-6596/1037/7/072037`

[4] Boorsma K and Caboni M 2020 Numerical analysis and validation of unsteady aerodynamics for floating offshore wind turbines Tech. Rep. R11345 TNO URL https://repository.tudelft.nl/islandora/object/uuid%3A10b69f85-dd5a-4f74-ac68-fdc62c01ead3
[5] Cormier M, Caboni M, Lutz T, Boorsma K and Krämer E 2018 *Journal of Physics: Conference Series* **1037** 072048 URL https://doi.org/10.1088/1742-6596/1037/7/072048
[6] Leishman J G 2002 *Wind Energy* **5** 85–132 URL https://doi.org/10.1002/we.62
[7] Yang L, Xie C and Yang C 2020 *Proceedings of the Institution of Mechanical Engineers, Part G: Journal of Aerospace Engineering* **234** 742–759 URL https://doi.org/10.1177/0954410019885238
[8] Gennaretti M, Bernardini G, Serafini J and Romani G 2018 *Aerospace Science and Technology* **80** 232–246 ISSN 1270-9638 URL https://doi.org/10.1016/j.ast.2018.07.013
[9] Sessarego M, Ramos-García N and Shen W 2015 *Journal of Power and Energy Engineering* **3** 1–6 URL https://doi.org/10.4236/jpee.2015.37001
[10] Wang L, Liu X and Kolios A 2016 *Renewable and Sustainable Energy Reviews* **64** 195–210 ISSN 1364-0321 URL https://doi.org/10.1016/j.rser.2016.06.007
[11] Gennaretti M and Bernardini G 2007 *AIAA Journal* **45** 1169–1176 URL https://doi.org/10.2514/1.18383
[12] Baayen J H 2012 *arXiv* URL https://doi.org/10.48550/arXiv.1210.6956
[13] Katz J and Plotkin A 2001 *Low-Speed Aerodynamics* 2nd ed Cambridge Aerospace Series (Cambridge University Press)
[14] Maskew B 1987 Program VSAERO theory document: A computer program for calculating nonlinear aerodynamic characteristics of arbitrary configurations Contractor Report 4023 National Aeronautics and Space Administration URL https://ntrs.nasa.gov/citations/19900004884
[15] Youngren H, Bouchard E, Coopersmith R and Miranda L 1983 *Comparison of panel method formulations and its influence on the development of QUADPAN, an advanced low-order method* URL https://doi.org/10.2514/6.1983-1827
[16] Anderson W K and Bonhaus D L 1994 *Computers & Fluids* **23** 1–21 ISSN 0045-7930 URL https://doi.org/10.1016/0045-7930(94)90023-X
[17] Sozer E, Brehm C and Kiris C C 2014 *52nd Aerospace Sciences Meeting* (AIAA) URL https://doi.org/10.2514/6.2014-1440
[18] Bernardini G, Serafini J, Molica Colella M and Gennaretti M 2013 *Aerospace Science and Technology* **29** 175–184 ISSN 1270-9638 URL https://doi.org/10.1016/j.ast.2013.03.002
[19] Theodorsen T 1934 General theory of aerodynamic instability and the mechanism of flutter Tech. Rep. 496 NACA URL https://digital.library.unt.edu/ark:/67531/metadc53413/
[20] Hand M, Simms D, Fingersh L, Jager D, Cotrell J, Schreck S and Larwood S 2001 Unsteady aerodynamics experiment phase VI: Wind tunnel test configurations and available data campaigns Tech. Rep. TP-500-29955 NREL URL https://doi.org/10.2172/15000240
[21] Masson C, Johansen J, Sørensen N, Zahle F, Bak C, Madsen H, Politis E, Schepers G, Lindenburg K, Snel H, Rooij R, Arens E, van Bussel G, Kuik G, Meng F, Sant T, Knauer A, Moe G, Munduate X and Schreck S 2008 IEA wind annex XX: HAWT aerodynamic and models from wind tunnel measurements - final report Tech. Rep. TP-500-43508 NREL URL https://www.nrel.gov/docs/fy09osti/43508.pdf
[22] Potsdam M A and Mavriplis D J 2009 *47th AIAA Aerospace Sciences Meeting including The New Horizons Forum and Aerospace Exposition* URL https://doi.org/10.2514/6.2009-1221
[23] Ribeiro A F P 2012 *Otimização e dinâmica dos fluidos computacional aplicadas a turbinas eólicas* Master's thesis Universidade Federal do Rio Grande do Sul URL http://hdl.handle.net/10183/60650
[24] Bayati I, Belloli M, Bernini L, Mikkelsen R and Zasso A 2016 *Journal of Physics: Conference Series* **753** 022028 URL https://doi.org/10.1088/1742-6596/753/2/022028
[25] Fontanella A, Bayati I, Mikkelsen R, Belloli M and Zasso A 2021 UNAFLOW: UNsteady Aerodynamics of FLOating Wind turbines URL https://doi.org/10.5281/zenodo.4740006
[26] Stern F, Wilson R V, Coleman H W and Paterson E G 2001 *Journal of Fluids Engineering* **123** 793–802 ISSN 0098-2202 URL https://doi.org/10.1115/1.1412235
[27] Mancini S, Boorsma K, Caboni M, Cormier M, Lutz T, Schito P and Zasso A 2020 *Wind Energy Science* **5** 1713–1730 URL https://doi.org/10.5194/wes-5-1713-2020
[28] Ramasamy M and Leishman J G 2007 *Journal of the American Helicopter Society* **52** 214–223 ISSN 2161-6027 URL https://doi.org/doi:10.4050/JAHS.52.214
[29] Tran T T and Kim D H 2016 *Renewable Energy* **90** 204–228 ISSN 0960-1481 URL https://doi.org/10.1016/j.renene.2015.12.013